

# Late-blooming magnetars: awakening as ultra-long period objects after a dormant cooling epoch

Arthur G. Suvorov<sup>†,1,2</sup> Clara Dehman<sup>†,1,\*</sup> and José A. Pons<sup>1</sup>

<sup>1</sup>*Departament de Física Aplicada, Universitat d'Alacant, Ap. Correus 99, E-03080 Alacant, Spain*

<sup>2</sup>*Theoretical Astrophysics, Eberhard Karls University of Tübingen, Tübingen 72076, Germany*

(Dated: May 9, 2025)

Ultra-long period transients (ULPs) are an elusive class of compact objects uncovered by radio surveys. While magnetars are a leading candidate for isolated ULPs, several observational properties challenge the established evolutionary framework: (i) low quiescent X-ray luminosities, (ii)  $\sim$  hour-long rotational periods, and (iii) highly-variable radio flux. It is shown via magnetothermal modelling that, if electric currents thread the fluid core at the time of crust freezing, the neutron star remains multiband silent for an initial period of approximately 0.1 Myr while cooling passively. Once the crust becomes cold enough, the Hall effect begins to dominate the magnetic evolution, triggering crustal failures that inject magnetospheric twist that initiates radio pulsing while depleting rotational kinetic energy from an already-slow star. Depending on where electric currents circulate, such ‘late-blooming’ magnetars manifesting as Galactic ULPs may thus form a distinct branch from soft gamma repeaters and anomalous X-ray pulsars.

## I. INTRODUCTION

Radio surveys are steadily revealing a Galactic population of astrophysical bodies termed ‘ultra-long period objects’ (ULPs) [14, 20, 49]. Although a robust classification for this burgeoning class is yet to emerge, coherent radio pulsations from  $\sim$  10 ULPs have been detected since the discovery of GLEAM-X J162759.5–523504 (GX J1627) [18]. Optical spectroscopy has established that some ULPs are white dwarfs with type M companions [19, 41]. However, whether *all* ULPs contain dwarfs remains debated, as neutron stars – particularly magnetars – are compelling candidates for those lacking binary signatures [28, 39, 43] or exhibiting interpulse phenomena [24].

The neutron-star hypothesis has garnered further support following the discovery of DART/ASKAP J1832–0911 (henceforth DA J1832) [25, 49]. This transient, with a period of  $P \approx 44.2$  min, was detected simultaneously in the radio and X-ray bands by a host of instruments between December 2023 and September 2024, a discovery enabled by its serendipitous alignment with the supernova remnant G22.7–0.2. This marked the first instance of such multiwavelength activity – characteristic of transient magnetars that become radio-loud during high-energy outbursts [46] – in a ULP. On the other hand, interpreting the source as a dwarf is challenging due to its high radio luminosity ( $L_{\text{rad,max}} \sim 10^{32}$  erg s<sup>−1</sup>) which requires field strengths exceeding those of any observed magnetic polar, assuming a relativistic cyclotron-maser emission mechanism [37].

Aside from the X-rays observed from DA J1832, isolated ULPs share a number of traits which have thus far eluded theoretical models. They are: (1) cold — deep X-ray follow-up on the first-discovered member of the class, GX J1627, set a stringent upper limit  $L_X \lesssim 2 \times 10^{30}$  erg s<sup>−1</sup> [39]; (2) slow — the current record-holder, ASKAP J183950.5–075635.0 (A J1839), has a period of  $P \approx 6.45$  hr [24]; and (3) irregularly active with low duty cycles — DA J1832 appears to have been radio-loud for only a few months in the past decade [49]. Despite the appeal of the magnetar model, reconciling all these properties within a single framework is challenging. Galactic magnetars are categorically hot [9] and magnetic decay is expected to restrict high-energy activity to early evolutionary stages, limiting their longevity to spin periods of at most  $\sim 20$  s [35].

Because the electrical conductivity of the fluid core significantly exceeds that of the crust, the effective magnetic diffusion timescale is extended if currents are primarily confined within the core. Even if the star boasts a large-scale field commensurate with magnetar strengths, coldness arises naturally in such a ‘core-threading’ (CT) scenario as field decay is stalled thereby preserving a strong field and limiting Joule heating during the star’s adolescence ( $\lesssim 0.1$  Myr) [12]. Eventually, however, the crust cools enough that Hall drift, a process in which field lines are advected by relative electron-ion motions, can start to efficiently redistribute magnetic energy. Sporadic radio activity then emerges as magnetic stresses induce crustal failures, twisting external field lines and increasing the voltage drop in magnetospheric gaps [1, 8]. Once the magnetospheric twist dissipates, the star returns to quiescence until the next outburst; the pulsar’s duty cycle may thus be regulated by event recurrence.

Observations indicate that magnetars typically slow down after outbursts [7, 27], likely due to previously closed field-lines being forced open by plasmoid ejection or otherwise pushed through the light cylinder [2, 44]. We show that, if even a modest fraction ( $\gtrsim 0.1\%$ ) of

\* clara.dehman@ua.es

† These authors are to be considered equal contributors.

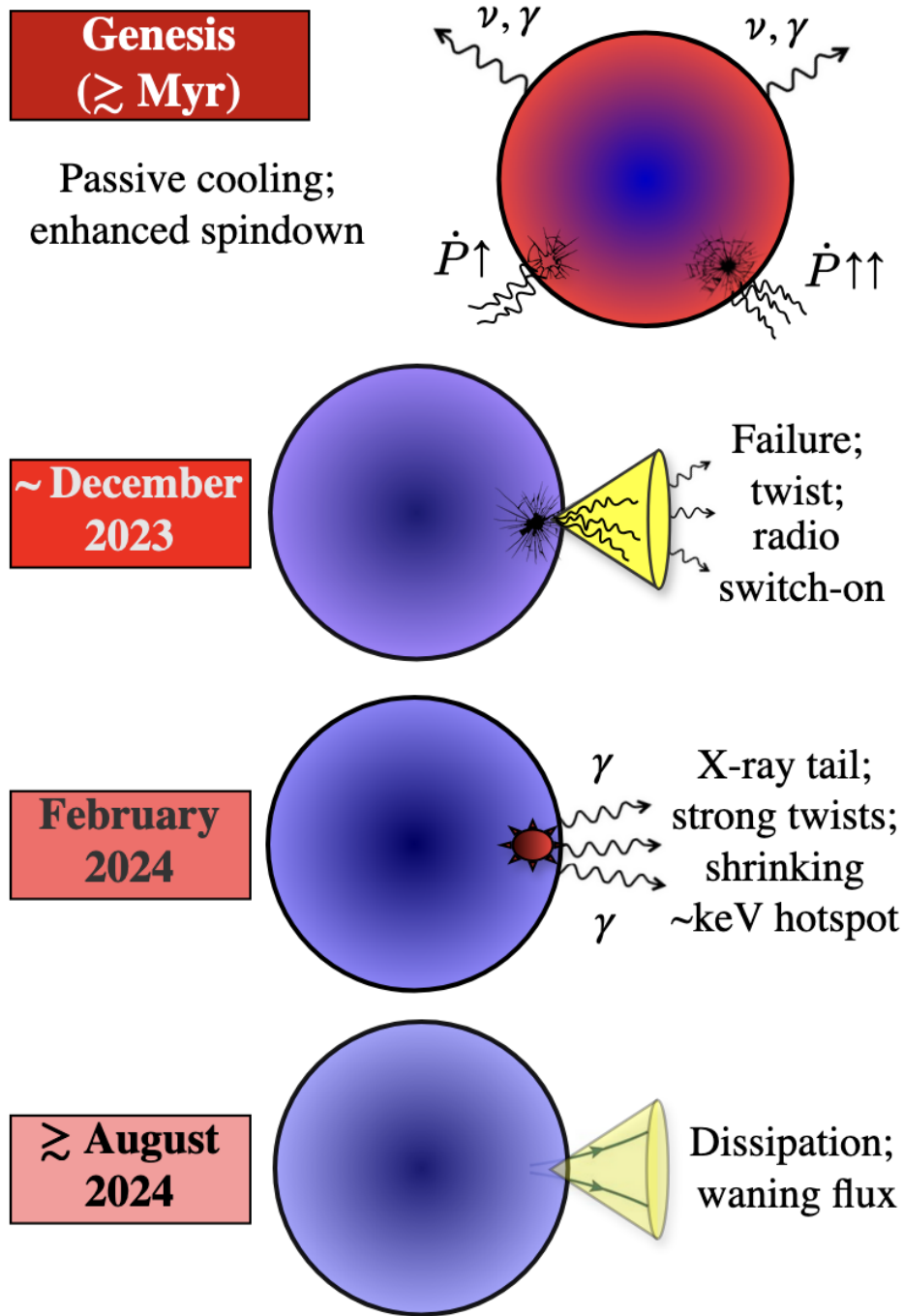


FIG. 1. Proposed timeline of DA J1832. (i) A silent era of neutrino and photon cooling whereby the electrical conductivity gradually increases, eventually instigating late-time activity and rapid spindown; (ii) crustal failure event in December 2023 and onset of radio pulsing; (iii) X-ray dissipation of the spot, the tail of which was observed in February 2024; (iv) twist decay and eventual shutoff.

the cumulative magnetoelastic energy release contributes to spindown, long periods ( $\sim$  hours) can be achieved at  $\sim$ Myr ages for CT models because the rotational kinetic energy is already low when the star activates magnetically. By contrast, crust-confined (CC) models – which better represent Galactic magnetars – fail often but early ( $\ll 0.1$  Myr), depleting magnetic energy [11, 33].

To demonstrate the proposed paradigm of ULPs as isolated magnetars we focus on DA J1832, whose observational timeline is summarised in Fig. 1. While DA J1832 is the only (isolated) ULP with an X-ray detection, this could reflect observational limitations rather than an intrinsic rarity, as shallow bursts capable of triggering radio emission impose narrow activity windows

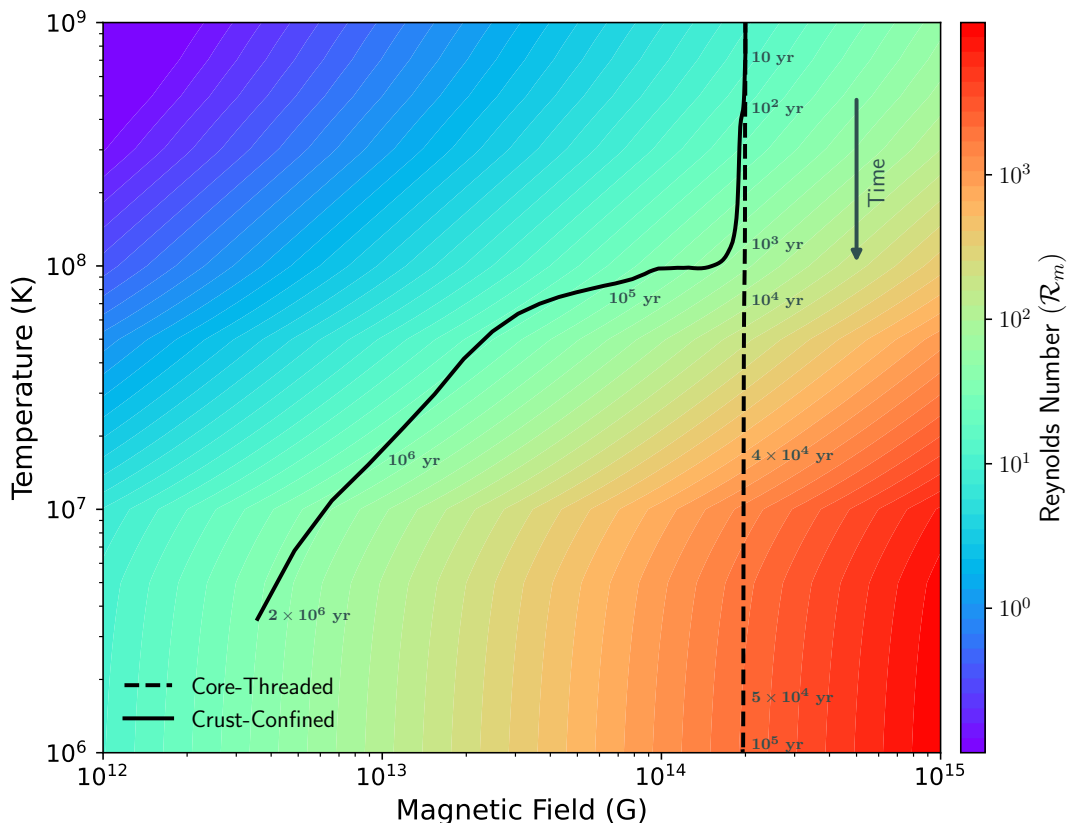


FIG. 2. Evolutionary tracks, in the  $T_b$ - $B_p$  plane, for the CC (solid) and CT (dashed) models. Stellar age is indicated by grey labels along the lines. The background colour contours show the magnetic Reynolds number ( $\mathcal{R}_m$ ), calculated at a density of  $\rho \approx 5 \times 10^{10}$  g/cm<sup>3</sup> for polar latitude, with redder shades indicating greater  $\mathcal{R}_m$ . Typically, the transition to a Hall-dominated epoch occurs when a track enters or neighbours the bottom-right quadrant.

and many ULPs have been identified only in archival data. We therefore expect this ‘late-blooming magnetar’ scenario to apply more broadly and anticipate future campaigns with contemporaneous X-ray and radio monitoring to test this picture.

## II. PRESERVING A STRONG FIELD TO FUEL LATE-TIME ACTIVITY

We evolve the magnetic and thermal fields of a neutron star over Myr-scales using a refined version of a well-tested magnetothermal code [47] (see Appendix A). The dynamics in the crust, which determines the shortest timescales, are governed by a generalised induction equation within the ‘electron-MHD’ regime [36]

$$\frac{\partial \mathbf{B}}{\partial t} = -\nabla \times \left\{ \eta \left[ \nabla \times \mathbf{B} + \mathcal{R}_m (\nabla \times \mathbf{B}) \times \hat{\mathbf{B}} \right] \right\}, \quad (1)$$

where  $\eta$  is the magnetic diffusivity and  $\mathcal{R}_m$  is the key plasma parameter – analogue to the magnetic Reynolds number in resistive magnetohydrodynamics – that dictates the evolutionary track. It is defined as the ratio

between Ohmic ( $\tau_\Omega$ ) and Hall ( $\tau_H$ ) timescales, viz.

$$\mathcal{R}_m = \frac{\tau_\Omega}{\tau_H} = \frac{L^2/\eta}{4\pi en_e L^2/cB} = \frac{cB}{4\pi en_e \eta}, \quad (2)$$

for magnetic length-scale  $L$ , speed of light  $c$ , elementary charge  $e$ , and electron number-density  $n_e$ . Relativistic corrections are implicitly accounted for in equation (1) via the gradient operator. Only when  $\mathcal{R}_m \gtrsim 10^2$  do Hall-related phenomena – where magnetic energy transfers between small and large scales – operate [13, 47]. These nonlinear cascades induce stress by driving flux waves that drift into malleable regions of the outer crust.

We consider two representative examples throughout, featuring poloidally-dominated, large-scale magnetic fields with an average strength of  $\gtrsim 10^{14}$  G that are nearly identical with respect to physical parameters (e.g. total magnetic energy, mass and radius, multipolarity, and poloidal-toroidal partition). The key distinction lies in the initial location of electric currents (CC or CT), highlighting the role of circulatory motions. This seemingly gentle change leads to fundamentally different evolutionary pathways: Fig. 2 shows their numerically-determined (solving equation 1 together with that of heat-balance) temperature–field–strength tracks. The

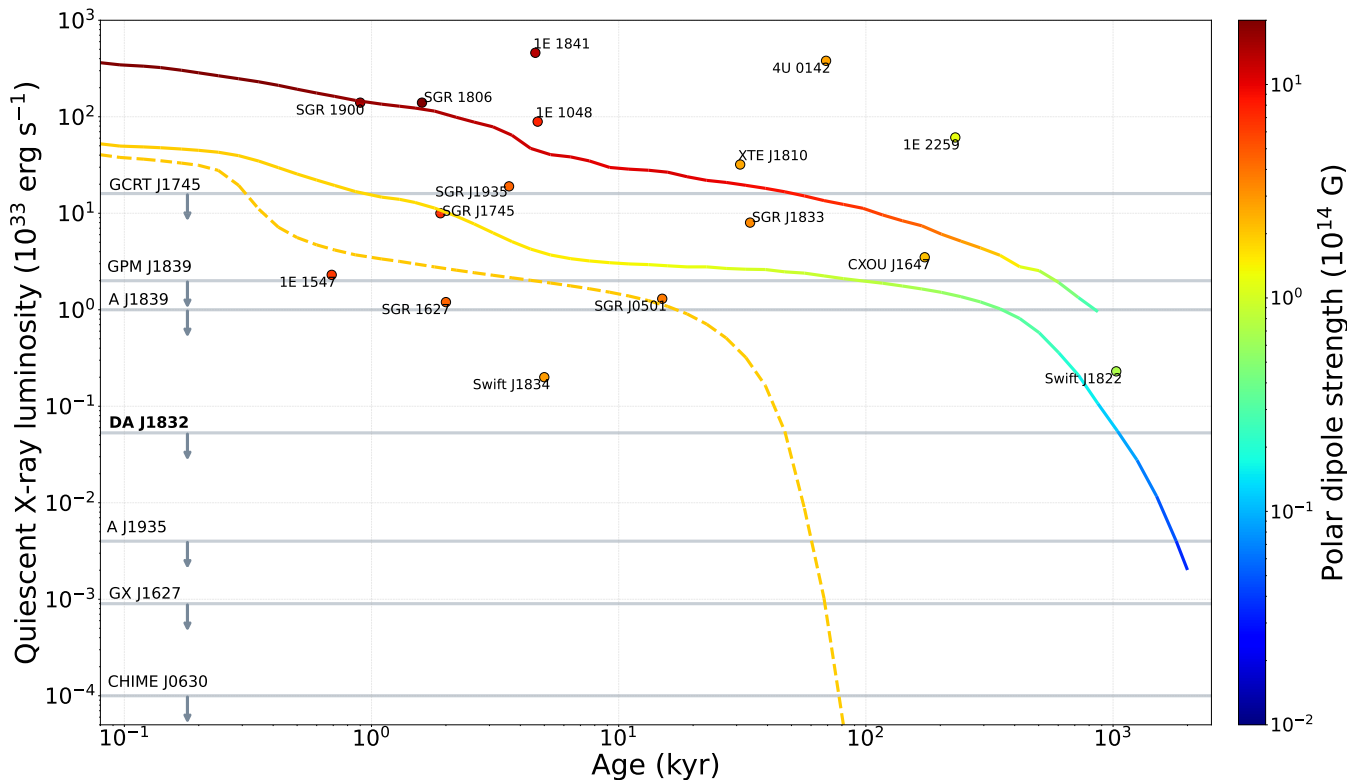


FIG. 3. Comparison of simulated (lines) and observed (points) luminosities for magnetars and ULPs. Solid (CC) and dashed (CT) tracks represent the X-ray luminosity curves as a function of the ‘real’ age as determined by the simulation. For the CC models, results are shown for two initial field strengths of  $2 \times 10^{14}$  G (lower) and  $2 \times 10^{15}$  G (upper). The color bar indicates the polar magnetic field intensity. Galactic magnetars are represented by circles as a function of their characteristic age. For seven isolated ULPs, upper limits on the X-ray luminosity are marked by the vertical arrows as reliable age estimates are unavailable for these objects.

overlaid colours depict the magnetic Reynolds number (2) with both, initially-hot models beginning in the top-right of the diagram. The CT track (dashed line) descends vertically, reflecting cooling with minimal magnetic activity until late times. In contrast, the CC model (solid line) diverts within  $\sim 10^2$  yr from this dive, evolving toward the bottom-left as the field decays in unison with cooling.

### A. X-ray dimness

The evolution of temperature at the base of the envelope,  $T_b$ , shown in Fig. 2, can be related to the surface temperature,  $T_s$ , assuming radiative equilibrium [16] (see Appendix A). Tracing  $T_s$  allows us to determine the X-ray luminosity as a function of age.

Fig. 3 shows the resulting (redshifted) luminosity curves, overlaid with the observed populations of isolated magnetars [9] and ULPs (see Appendix B and Ta-

ble I). Notably, we do not have reliable information to estimate ULP ages: there are only upper limits to  $\dot{P}$ , and the dipole braking formula is not applicable. For CT (dashed curve), the quiescent X-ray luminosity drops below  $L_X \sim 10^{30}$  erg s $^{-1}$  within  $\lesssim 0.1$  Myr. For CC (solid) models, we show results for two models with the same structure but distinct initial polar-dipole strengths ( $2 \times 10^{14}$  G and  $2 \times 10^{15}$  G), the larger of which better matches the Galactic magnetar track. In both cases, the luminosity only dips to GX J1627-like values after  $\gtrsim 2$  Myr. Importantly though, the field has decayed sufficiently at that point so as to disable failure activity.

### B. Failure rates, radio activation, and pulsar duty cycle

Mechanical stresses accumulate in an elastic crust as a strong ( $\gtrsim 10^{14}$  G) magnetic field evolves [3, 44]. If a critical strain threshold, which depends on the crustal

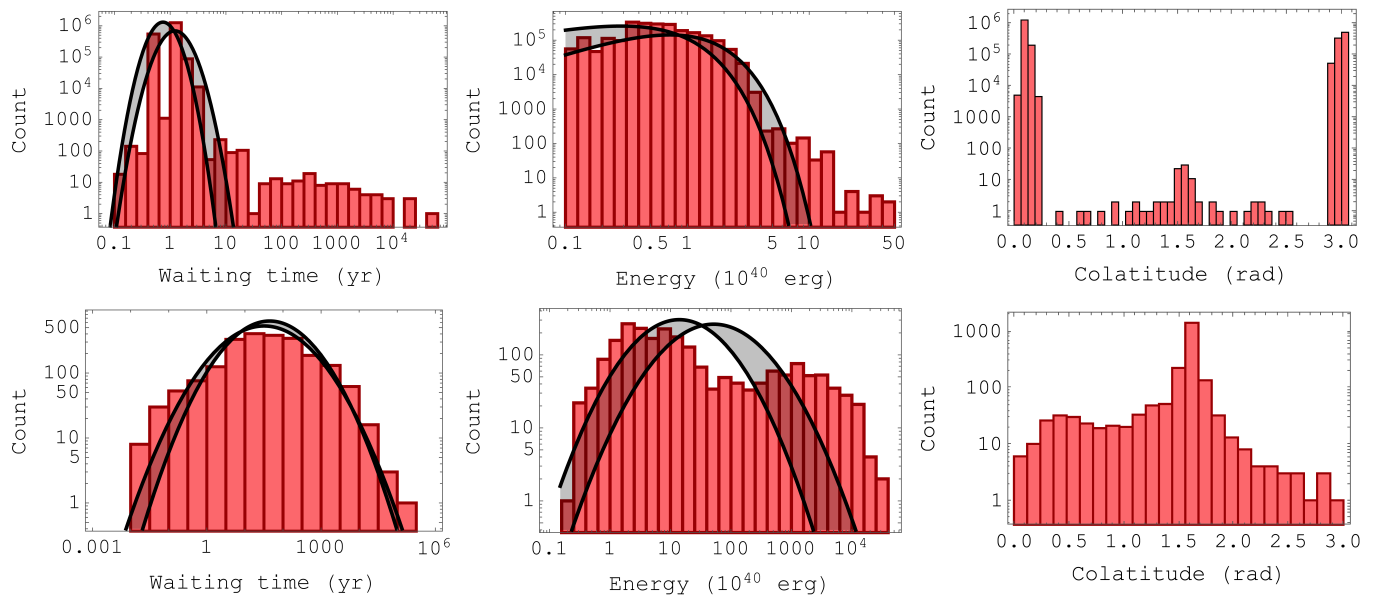


FIG. 4. Histograms of waiting times (left), energies (middle), and colatitudes (right) of failure events counted during evolution for the representative CT (top panel) and CC (bottom) models up to ages  $\tau = 2$  Myr and  $\tau = 1.375$  Myr, respectively. Maximum-likelihood and method of moments fits, log-normal for both sets of waiting times, are overlaid with uncertainties. For the energy distributions, a gamma (log-normal) fit best represents the simulation output for model CT (CC).

particulars, is breached during a Hall-dominated era, a *failure* can occur [10]. By tracking stresses, we can identify failure sites (see Sec. A 1). Relevant statistical properties of our two representative cases are given in Fig. 4 for CT (top) and CC (bottom). We show the waiting time distribution of events (left), the energy released per failure (middle), and the colatitudes of failure sites (right). The CC waiting-time distribution clearly follows a log-normal shape, consistent with prolific magnetars like SGR 1806–20 [15], where ample burst statistics are available.

How exactly failures manifest is poorly understood. Because of the immense hydrostatic pressures, however, it is thought that, rather than shattering like glass as brittle material would, failed regions deform plastically and flow for a duration that depends on the (unknown) kinematic viscosity of nucleon-rich matter [21]. Notably, fluid circulating within ‘plastic islands’ surrounding failure sites (at speeds which may exceed  $\sim 10^3$  cm yr $^{-1}$  [23]) constitutes an effective longitudinal velocity which, via induction, produces an electric field that may work to accelerate charges to high-enough Lorentz factors, initiating pair cascading and triggering radio activity for [8]  $B \gtrsim 10^{14}$  G. One can think of this as a localised rotation which dominates over rigid rotation for ULPs. In particular, traditional radio activation theory demands a minimum voltage to excite the necessary pair multiplicity which is difficult to achieve for ULPs unless  $B \gg 10^{14}$  G because  $P$  is so large [43].

ULPs frequently null, often displaying duty cycles on the order of  $D \sim 1\%$  (see Table I). Plastic velocities depend on the viscosity which is likely sensitive to the

temperature and density of the failed region, and thus plastic phases may vary in duration from source to source depending on age and field strength. Even without a quantitative estimate for the viscosity though, we note that for CT – the proposed ULP track – the waiting time distribution peaks at  $\sim 1$  yr, and thus if motions circulate in a plastic island for  $\sim 6$  months (as anticipated from the radio continuity of [49] DA J1832), we estimate an upper limit  $D_{\max} \sim 0.5$ . On the other hand, beaming and inclination elements will reduce this factor to a point that could accommodate sub-percent cycles, such as that observed from CHIME J0630+25 (Tab. I). For example, if only failures occurring at a narrow range of co-latitudes surrounding  $\theta \sim 0.3$  rad are visible due to inclination [38], the right panel of Fig. 4 indicates that only 1 in  $\gtrsim 10^2$  events may reveal in radio. This gives  $D \lesssim 1\%$ , more in line with observations of GX J1627 or ASKAP J1935+2148; see Tab. I.

The colatitude distribution of failure sites is bimodal at polar angles. This is in agreement with hotspot observations of DA J1832: a significant phase overlap between the 1–10 keV flux and radio pulsing was observed in February 2024 [49], suggestive that the pulsed component of the X-rays was spatially coincident with the radio emission zone, and thus that a hotspot resided near the magnetic dipole axis. Related arguments have been made for events from XTE J1810–197 [2], which bears similarity to the ULP GPM J1839 [31]. Our simulations further indicate that Hall drift frequently induces failures at *both* polar caps in rapid succession, naturally explaining interpulse observations of A J1839 with two diametrically opposed plastic islands [24].

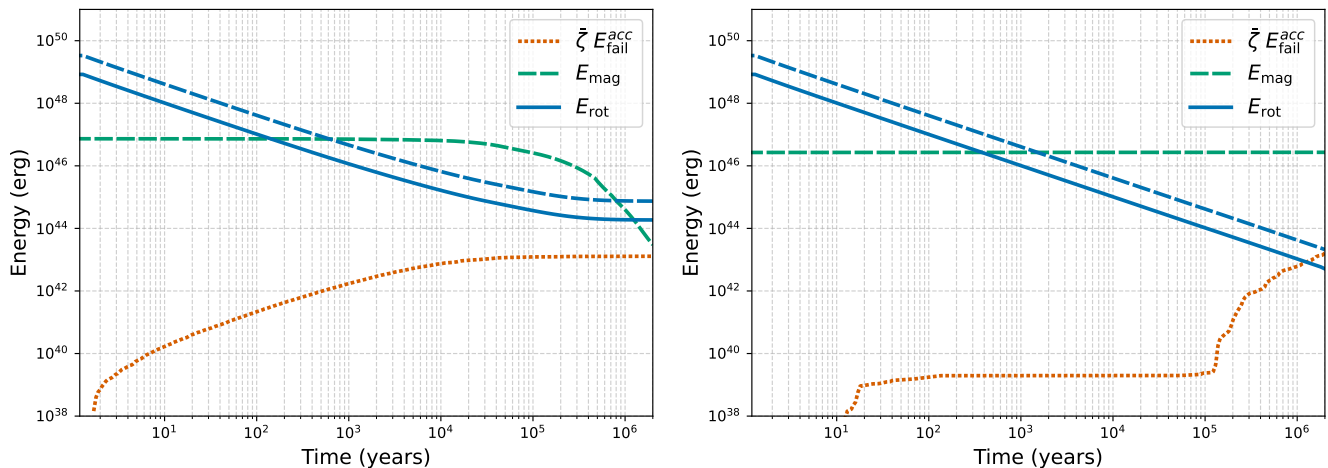


FIG. 5. Time evolutions of the normalised ( $\bar{\zeta} = 10^{-3}$ ) cumulative failure (dotted red), magnetic ( $E_{\text{mag}}$ , dashed green), and rotational ( $E_{\text{rot}}$ , blue) energies for representative CC (left) and CT (right) cases. The solid (dashed) blue curve corresponds to equation (3) for an orthogonal (aligned) rotator.

Energy distributions for CT imply that most failure events should be dim: if only  $\sim 1\%$  of the failure energy converts to observable X-rays [5], most bursts would fall below detection thresholds. This could explain why only DA J1832 has shown coincident X-ray and radio activity. We stress again, however, that several ULPs were discovered in archival data, and thus X-ray follow-up some years after radio activation is inappropriate to assess the scenario proposed here. Furthermore, the best-fit gamma distribution for CT energetics hints at buildup, where multiple sub-events may be required to trigger ‘major’ failures. For DA J1832, the pulsed component was brighter than the ambient blackbody, meaning weak bursts might not significantly raise the overall temperature, keeping them below detection limits for many ULPs despite their potential to ignite electron-positron cascades.

### III. ENHANCED SPINDOWN VIA LATE-TIME BURSTING

Suppose that  $P(t)$  evolves following that of a dipolar, inclined rotator

$$P\dot{P} = \frac{2\pi^2 B_p^2 R^6}{3c^3 I_0} \lambda(\alpha), \quad (3)$$

for magnetic inclination angle  $\alpha$  and (time-dependent) polar-dipole strength  $B_p$ . The order-unity factor  $\lambda$  encapsulates drag due to the magnetospheric conditions; for a star surrounded by self-sourced plasma  $\lambda \approx 1 + \sin^2 \alpha$  [42]. Since orthogonality is supported in neutron-star ULPs by interpulse observations of A J1839 [24], we set  $\alpha = \pi/2$ .

However, magnetars and high-B pulsars invariably enter into phases of accelerated spindown following out-

bursts [44]. This is expected theoretically as twists imparted by crustal failures work to drive winds and inflate magnetospheric field lines. Such effects likely depend on complicated preexisting magnetospheric (e.g. multipoles) structure and on the nature of the failure itself (e.g. latitude and depth). This could explain why, although hard X-ray emission and spindown in Galactic magnetars is strongly correlated, relationships between burst energetics and timing residuals vary from source to source [45].

Such a relationship can be quantified phenomenologically by an *efficiency*,  $\bar{\zeta}$ , relating the energy of a given failure to rotational kinetic energy losses, viz.

$$\Delta E_{\text{rot}} = -\bar{\zeta} E_{\text{failure}}, \quad (4)$$

where  $E_{\text{rot}} = 2\pi^2 I_0 / P^2$  for moment of inertia  $I_0 \sim 10^{45} \text{ g cm}^2$ . Based on magnetospheric transmission theory [4, 26], global quake simulations [5], and observations [7, 27], we argue that  $\bar{\zeta} \sim 10^{-3}$  is reasonable (see Appendix C). Fig. 5 presents time evolutions for the cumulative failure energy (dotted), magnetic energy (dashed), and rotational kinetic energy (thick band) for CC (left panel) and CT (right) configurations. The thickness of the band accounts for uncertainties in magnetospheric drag. The cumulative failure energy is scaled by  $\bar{\zeta} = 10^{-3}$ . Note that for the CT model, the baseline  $B_p$  is almost constant over the first  $\sim 2 \text{ Myr}$  (see the green curve in Fig. 5).

For CC cases, magnetic decay occurs at  $\ll \text{Myr}$  ages whereupon crustal failures, which were otherwise continuously excited, halt. Note in particular that towards the end of the simulation, the magnetic energy in the CC model approaches the cumulative failure energy so that magnetic activity should shut off completely and no further spindown enhancement can occur. At this stage, the efficiency-corrected, cumulative failure energy remains approximately two orders of magnitude lower than the

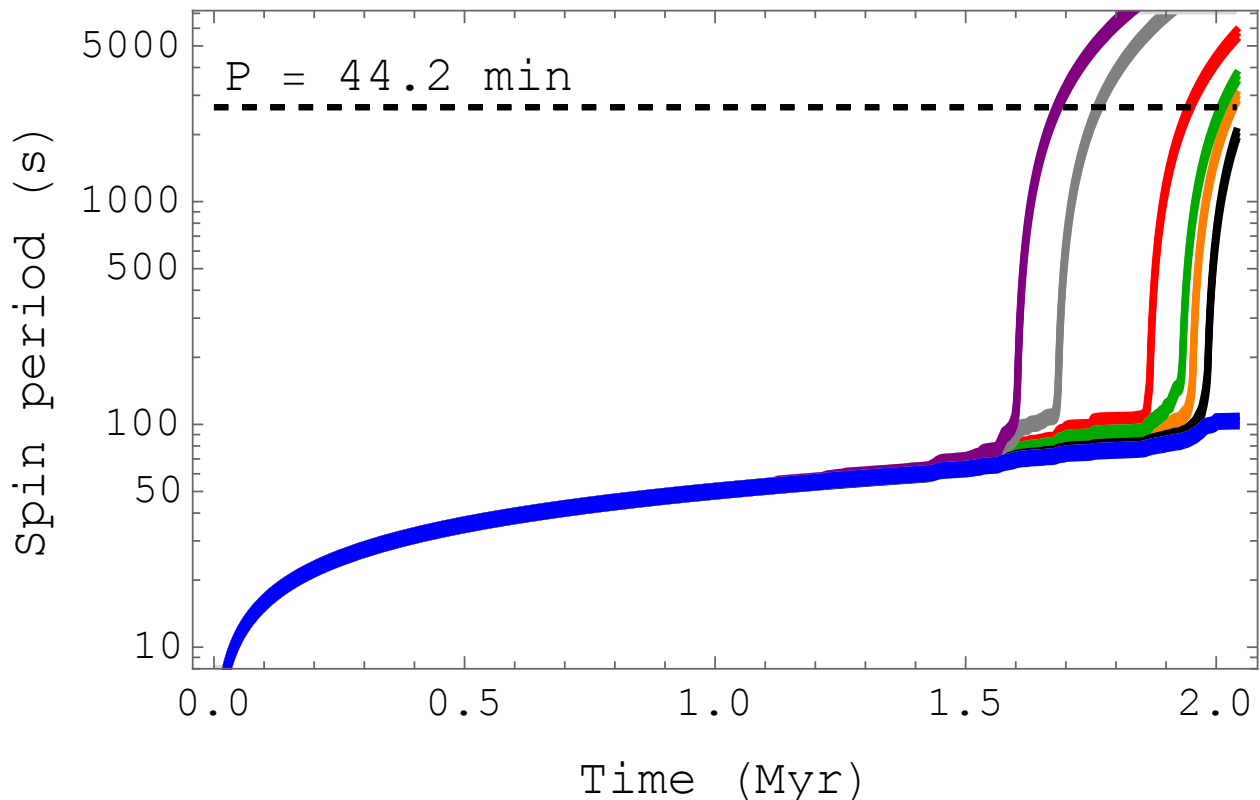


FIG. 6. Realisations of spindown trajectories for the CT model with various efficiencies spanning the range  $7 \leq \bar{\zeta}/(10^{-4}) \leq 14$  in increments of  $10^{-4}$  (with  $\bar{\zeta}$  increasing from left to right). The spin period of DA J1832 ( $P \approx 44.2$  min) is overlaid by the dashed, horizontal line. Models with  $\bar{\zeta} \gtrsim 8 \times 10^{-4}$  are sufficiently slow by  $\tau \sim 2$  Myr to match the observed pulse period.

rotational energy, implying that adolescent activity cannot allow the system to mature with a long period. While CC models dominated by small-scales and stronger fields overall can better explain X-ray observations of Galactic magnetars (Fig. 3), they fare worse in terms of explaining ULPs. This is because, even though  $\mathcal{R}_m \propto B$  is itself independent of the system length-scale, both the Hall and Ohmic times scale as  $L^2$  which is smaller for multipoles (equation 2). This prevents *any* CC model from reaching ULP-like periods even if  $P \sim 10$  s earlier in life due to plentiful Hall activity [35]. In CT simulations by contrast failures only start taking place en masse when  $P \sim 10$  s and  $\mathcal{R}_m \gtrsim 100$ . Around  $\gtrsim 1$  Myr, the cumulative failure energy becomes comparable to the rotational energy for  $\bar{\zeta} \approx 10^{-3}$ , indicating that injected twists could effectively drain the entire rotational kinetic energy reservoir.

Thus far we have treated spindown by appealing only to energetics. A physical model can instead be considered where, when a failure event is triggered, the dipole moment in (3) is increased over a short rise-time by a factor (assumed constant across events for simplicity) proportional to the event energy. The boosting factor is normalised such that  $\dot{P}$  is always bounded by the observational limit, viz.  $\dot{P} < 10^{-9} \text{ ss}^{-1}$  [49]. The twist is diffused linearly – in rough agreement with magnetar observations [46] – over a timescale which is fixed consis-

tently by enforcing (4) as an integral condition. A set of realisations following this method, using the distributions shown in Fig. 4, is shown in Fig. 6 for  $0.07\% \leq \bar{\zeta} \leq 0.14\%$  in increments of 0.01% (right to left). For  $\bar{\zeta} \gtrsim 0.08\%$ , we see that the spindown enhancement induced by failures is sufficient to slow the object to periods consistent with DA J1832. Furthermore, anticipating that magnetic field strengths and the average  $\bar{\zeta}$  may vary by a factor of a few between sources, a wide range of spin periods, from several minutes to multiple hours, can be explained for ages  $\gtrsim$  Myr.

#### IV. PREDICTIONS AND IMPLICATIONS FOR THE ULP POPULATION

It has been shown that the defining characteristics of isolated ULPs (focussing in particular on recent multi-band observations of DA J1832; Fig. 1) can be explained with a magnetar model ( $B \gtrsim 10^{14}$  G) provided that electrical currents circulate through the core. This assumption alters the star’s trajectory in the temperature-field phase space, as illustrated in Fig. 2 depicting the magnetic Reynolds number. Our simulations show that  $\mathcal{R}_m \gtrsim 10^2$  at  $\gtrsim 0.1$  Myr ages, whereupon the star is cold ( $T_s \lesssim 10^6$  K) and too dim to be observable in

X-rays (Fig. 3). At this age, it enters into a delayed Hall-dominated epoch such that it effectively reawakens as what we have called a ‘late-blooming magnetar’ that can display high-energy activity seeded by crustal failures (Fig. 4). Critically, rotational energy is already relatively low ( $\sim 10^{44}$  erg; Fig. 5) at this stage meaning that if even a fraction ( $\zeta \sim 10^{-3}$ ; Fig. 6) of the failure energy goes into spindown the star could reach a range of periods between many minutes and several hours. The radio duty cycle is tied to the failure statistics in this picture; given that the peak of the waiting-time distribution lies at  $\sim 1$  yr, we anticipate that  $D \sim \mathcal{O}(0.1)$  for systems with favourable viewing angles (as for GPM J1839). Interestingly, we also find that failure latitudes cluster around the poles, which naturally explains the polar latitude of the hotspot of DA J1832 [49] and inter-pulses from A J1839 [24].

A natural question to ask is *why* some objects may have core-threading fields and others not. Because of the high degree of degeneracy, protons within neutron-star cores are expected [17] to enter into a superconducting phase some time after birth. A general prediction in this scenario is that of an eventual Meissner state, where core magnetic flux is expelled into the crust. Such a setup is typically taken for granted in magnetothermal evolutions of magnetars [36], as for our CC model. However, it has been argued [22] that certain pre-condensation conditions may prevent a full or partial Meissner expulsion. Such differences, effectively established in the proto-phase based on the chemical stratification and convective velocity profile, may therefore decide whether a comparatively strong-field object follows the ULP or canonical magnetar track.

Stars hosting a predominantly large-scale field near the critical superconducting value,  $H_c \sim \text{few} \times 10^{14}$  G, may be more conducive to a core-threading geometry because the angular distance a field line must drift until it encounters an opposite-polarity line (i.e. setting a reconnection

timescale) is larger than that of a multipolar configuration [22]. Consequently, flux may be more easily pushed into the crust for stars with tangled fields — as anticipated for canonical magnetars. Hall waves of high amplitude may also be launched into the crust as flux is thrust there [6] either through a Meissner transition or ambipolar drift. Notably, waves of the low-frequency, whistler variety may enduringly propagate in latitudinal directions such that the ambient poloidal field oscillates violently, instigating intermittent heating, anomalous torques, avalanche phenomena, and multiband transients. Ab initio modelling in this direction could be used to pave the way for population synthesis studies of canonical vs. ‘late-blooming’ magnetars.

For completeness, and although a thorough exploration of alternate interpretations lies beyond the scope of this work, we highlight a number of observations that would be difficult to reconcile with the model put forward here. (1) Binary companions are detected. For example the absence of optical/NIR/UV measurements from DA J1832 does not necessarily indicate the absence of a companion owing to dust obscuration and the Galactic latitude of the source [25, 49]. Nevertheless, it seems probable that the source is an isolated magnetar owing to difficulties in explaining the observational characteristics with a dwarf-M interaction, notably the high radio luminosity [37]. For some other ULPs like GX J1627, multiband followup carried out since source discovery is much more decisive in ruling out binarity [28]. (2) A hot ULP is found. If a high-baseline X-ray flux is detected from a ULP, this would indicate youth and strong Joule currents, both of which would disfavour a late bloomer. (3) A fallback disk is detected. This would challenge the model here as it could remove the need for enhanced spindown [40] and one may argue for younger ULPs. Regardless, deeper multiwavelength limits will help to validate the scenario proposed here or otherwise; other important caveats are spelled out in Appendix A.

- 
- [1] Beloborodov, A. M. & Thompson, C. Corona of magnetars. *Astrophys. J.* **657**, 967–993 (2007).
  - [2] Beloborodov, A. M. Untwisting magnetospheres of neutron stars. *Astrophys. J.* **703**, 1044–1060 (2009).
  - [3] Beloborodov, A. M. & Levin, Y. Thermoplastic waves in magnetars. *Astrophys. J. Lett.* **794**, L24 (2014).
  - [4] Blaes, O., Blandford, R., Goldreich, P. & Madau, P. Neutron starquake models for gamma-ray bursts. *Astrophys. J.* **343**, 839 (1989).
  - [5] Bransgrove, A., Beloborodov, A. M. & Levin, Y. A quake quenching the Vela pulsar. *Astrophys. J.* **897**, 173 (2020).
  - [6] Bransgrove A., Levin Y., Beloborodov A. M., 2025, ApJ, 979, 144. doi:10.3847/1538-4357/ad90a3
  - [7] Borghese, A., Rea, N., Turolla, R., Rigoselli, M., Alford, J. A. J., Gotthelf, E. V., Burgay, M., Possenti, A., Zane, S., Coti Zelati, F., Perna, R., Esposito, P., Mereghetti, S., Viganò, D., Tiengo, A., Götz, D., Ibrahim, A., Israel, G. L., Pons, J. & Sathyaprakash, R. The X-ray evolution and geometry of the 2018 outburst of XTE J1810-197. *Mon. Not. R. Astron. Soc.* **504**, 5244–5257 (2021).
  - [8] Cooper, A. J. & Wadiasingh, Z. Beyond the rotational deathline: radio emission from ultra-long period magnetars. *Mon. Not. R. Astron. Soc.* **533**, 2133–2155 (2024).
  - [9] Coti Zelati, F., Rea, N., Pons, J. A., Campana, S. & Esposito, P. Systematic study of magnetar outbursts. *Mon. Not. R. Astron. Soc.* **474**, 961–1017 (2018).
  - [10] Chugunov, A. I. & Horowitz, C. J. Breaking stress of neutron star crust. *Mon. Not. R. Astron. Soc. Lett.* **407**, L54–L58 (2010).
  - [11] Dehman, C., Viganò, D., Rea, N., Pons, J. A., Perna, R. & Garcia-Garcia, A. On the rate of crustal failures in young magnetars. *Astrophys. J. Lett.* **902**, L32 (2020).
  - [12] Dehman, C., Pons, J. A., Viganò, D. & Rea, N. How bright can old magnetars be? Assessing the impact of magnetized envelopes and field topology on neutron star cooling. *Mon. Not. R. Astron. Soc.* **520**, L42–L47 (2023).



- [13] Dehman, C. & Brandenburg, A. Reality of inverse cascading in neutron star crusts. *A&A* **694**, A39 (2025).
- [14] Dong, F. A., Clarke, T., Curtin, A. P., Kumar, A., Stairs, I., Chatterjee, S., Cook, A. M., Fonseca, E., Gaensler, B. M., Hessels, J. W. T., Kaspi, V. M., Lazda, M., Masui, K. W., McKee, J. W., Meyers, B. W., Pearlman, A. B., Ransom, S. M., Scholz, P., Shin, K., Smith, K. M. & Tan, C. M. The discovery of a nearby 421 s transient with CHIME/FRB/Pulsar. *arXiv e-prints*, arXiv:2407.07480 (2024).
- [15] Göğüş, E., Woods, P. M., Kouveliotou, C., van Paradijs, J., Briggs, M. S., Duncan, R. C. & Thompson, C. Statistical properties of SGR 1806-20 bursts. *Astrophys. J. Lett.* **532**, L121–L124 (2000).
- [16] Gudmundsson, E. H., Pethick, C. J. & Epstein, R. I. Structure of neutron star envelopes. *Astrophys. J.* **272**, 286–300 (1983).
- [17] Haskell, B. & Sedrakian, A. Superfluidity and superconductivity in neutron stars. In Rezzolla, L., Pizzochero, P., Jones, D. I., Rea, N. & Vidaña, I. (eds.), *Astrophysics and Space Science Library*, 457, 401 (2018).
- [18] Hurley-Walker, N., Zhang, X., Bahramian, A., McSweeney, S. J., O’Doherty, T. N., Hancock, P. J., Morgan, J. S., Anderson, G. E., Heald, G. H. & Galvin, T. J. A radio transient with unusually slow periodic emission. *Nature (London)* **601**, 526–530 (2022).
- [19] Hurley-Walker, N., McSweeney, S. J., Bahramian, A., Rea, N., Horváth, C., Buchner, S., Williams, A., Meyers, B. W., Strader, J., Aydi, E., Urquhart, R., Chomiuk, L., Galvin, T. J., Coti Zelati, F. & Bailes, M. A 2.9 hr Periodic Radio Transient with an Optical Counterpart. *Astrophys. J. Lett.* **976**, L21 (2024).
- [20] Hurley-Walker, N., Rea, N., McSweeney, S. J., Meyers, B. W., Lenc, E., Heywood, I., Hyman, S. D., Men, Y. P., Clarke, T. E., Coti Zelati, F., Price, D. C., Horváth, C., Galvin, T. J., Anderson, G. E., Bahramian, A., Barr, E. D., Bhat, N. D. R., Caleb, M., Dall’Ora, M., de Martino, D., Giacintucci, S., Morgan, J. S., Rajwade, K. M., Stappers, B. & Williams, A. A long-period radio transient active for three decades. *Nature (London)* **619**, 487–490 (2023).
- [21] Jones, P. B. Bulk viscosity of neutron-star matter. *Phys. Rev. D* **64**, 084003 (2001).
- [22] Lander, S. K. The Meissner effect in neutron stars. *Mon. Not. R. Astron. Soc.* **535**, 2449–2468 (2024).
- [23] Lander, S. K. & Gourgouliatos, K. N. Magnetic-field evolution in a plastically failing neutron-star crust. *Mon. Not. R. Astron. Soc.* **486**, 4130–4143 (2019).
- [24] Lee, Y. W. J., Caleb, M., Murphy, T., Lenc, E., Kaplan, D. L., Ferrario, L., Wadiasingh, Z., Anumarlapudi, A., Hurley-Walker, N., Karambelkar, V. & others. The emission of interpulses by a 6.45-h-period coherent radio transient. *Nat. Astron.*, 1–13 (2025).
- [25] Li, D., Yuan, M., Wu, L., Yan, J., Lv, X., Tsai, C.-W., Wang, P., Zhu, W., Deng, L., Lan, A. & others. A 44-minute periodic radio transient in a supernova remnant. *arXiv e-prints*, arXiv:2411.15739 (2024).
- [26] Link, B., 2014, MNRAS, 441, 2676. doi:10.1093/mnras/stu584
- [27] Lower, M. E., Younes, G., Scholz, P., Camilo, F., Dunn, L., Johnston, S., Enoto, T., Sarkissian, J. M., Reynolds, J. E., Palmer, D. M. & others. The 2022 high-energy outburst and radio disappearing act of the magnetar 1E 1547.0-5408. *Astrophys. J.* **945**, 153 (2023).
- [28] Lyman J. D., Dhillon V. S., Kamann S., Chrimes A. A., Levan A. J., Pelisoli I., Steeghs D. T. H., et al., 2025, MNRAS.tmp. doi:10.1093/mnras/staf325
- [29] Marino, A., Dehman, C., Kovelakas, K., Rea, N., Pons, J. A. & Viganò, D. Constraints on the dense matter equation of state from young and cold isolated neutron stars. *Nat. Astron.* **8**, 1020–1030 (2024).
- [30] Mattana, F., Götz, D., Falanga, M., Senziani, F., de Luca, A., Esposito, P. & Caraveo, P. A. A new symbiotic low mass X-ray binary system: 4U 1954+319. *A&A* **460**, L1–L4 (2006).
- [31] Men Y., McSweeney S., Hurley-Walker N., Barr E., Stappers B., 2025, SciA, 11, eadp6351. doi:10.1126/sciadv.adp6351
- [32] Metzger, B. D., Beniamini, P. & Giannios, D. Effects of fallback accretion on protomagnetar outflows in gamma-ray bursts and superluminous supernovae. *Astrophys. J.* **857**, 95 (2018).
- [33] Perna, R. & Pons, J. A. A unified model of the magnetar and radio pulsar bursting phenomenology. *Astrophys. J. Lett.* **727**, L51 (2011).
- [34] Perna, R., Hernquist, L. & Narayan, R. Emission spectra of fallback disks around young neutron stars. *Astrophys. J.* **541**, 344–350 (2000).
- [35] Pons, J. A., Viganò, D. & Rea, N. A highly resistive layer within the crust of X-ray pulsars limits their spin periods. *Nat. Phys.* **9**, 431–434 (2013).
- [36] Pons, J. A. & Viganò, D. Magnetic, thermal and rotational evolution of isolated neutron stars. *Living Rev. Comput. Astrophys.* **5**, 3 (2019).
- [37] Qu Y., Zhang B., 2025, ApJ, 981, 34. doi:10.3847/1538-4357/adb1b5
- [38] Radhakrishnan V., Cooke D. J., 1969, ApL, 3, 225
- [39] Rea, N., Coti Zelati, F., Dehman, C., Hurley-Walker, N., de Martino, D., Bahramian, A., Buckley, D. A. H., Brink, J., Kawka, A., Pons, J. A., Viganò, D., Graber, V., Ronchi, M., Pardo Araujo, C., Borghese, A., Parent, E. & Galvin, T. J. Constraining the Nature of the 18 min Periodic Radio Transient GLEAM-X J162759.5-523504.3 via Multiwavelength Observations and Magneto-thermal Simulations. *Astrophys. J.* **940**, 72 (2022).
- [40] Ronchi, M., Rea, N., Graber, V. & Hurley-Walker, N. Long-period pulsars as possible outcomes of supernova fallback accretion. *Astrophys. J.* **934**, 184 (2022).
- [41] de Ruiter, I., Rajwade, K. M., Bassa, C. G., Rowlinson, A., Wijers, R. A. M. J., Kilpatrick, C. D., Stefansson, G., Callingham, J. R., Hessels, J. W. T., Clarke, T. E., Peters, W., Wijnands, R. A. D., Shimwell, T. W., ter Veen, S., Morello, V., Zeimann, G. R. & Mahadevan, S. A white dwarf binary showing sporadic radio pulses at the orbital period. *arXiv e-prints*, arXiv:2408.11536 (2024).
- [42] Spitkovsky, A. Time-dependent force-free pulsar magnetospheres: axisymmetric and oblique rotators. *Astrophys. J. Lett.* **648**, L51–L54 (2006).
- [43] Suvorov, A. G. & Melatos, A. Evolutionary implications of a magnetar interpretation for GLEAM-X J162759.5-523504.3. *Mon. Not. R. Astron. Soc.* **520**, 1590–1600 (2023).
- [44] Thompson, C., Lyutikov, M. & Kulkarni, S. R. Electrodynamics of magnetars: implications for the persistent X-ray emission and spin-down of the soft gamma repeaters and anomalous X-ray pulsars. *Astrophys. J.* **574**, 332–355 (2002).

- [45] Thompson, C., Yang, H. & Ortiz, N. Global crustal dynamics of magnetars in relation to their bright X-ray outbursts. *Astrophys. J.* **841**, 54 (2017).
- [46] Turolla, R., Zane, S. & Watts, A. L. Magnetars: the physics behind observations. A review. *Rep. Prog. Phys.* **78**, 116901 (2015).
- [47] Viganò, D., Garcia-Garcia, A., Pons, J. A., Dehman, C. & Graber, V. Magneto-thermal evolution of neutron stars with coupled Ohmic, Hall and ambipolar effects via accurate finite-volume simulations. *Comput. Phys. Commun.* **265**, 108001 (2021).
- [48] Wallner, A., Feige, J., Kinoshita, N., Paul, M., Fifield, L. K., Golser, R., Honda, M., Linnemann, U., Matsuzaki, H., Merchel, S., Rugel, G., Tims, S. G., Steier, P., Yamagata, T. & Winkler, S. R. Recent near-Earth supernovae probed by global deposition of interstellar radioactive  $^{60}\text{Fe}$ . *Nature (London)* **532**, 69–72 (2016).
- [49] Wang, Z., Rea, N., Bao, T., Kaplan, D. L., Lenc, E., Wadiasingh, Z., Hare, J., Zic, A., Anumalapudi, A., Bera, A. & others. Detection of X-ray Emission from a Bright Long-Period Radio Transient. *arXiv preprint*, arXiv:2411.16606 (2024).

## Appendix A: Magneto-thermal evolution

To describe the hydrostatics of the background state, we solve the Tolman-Oppenheimer-Volkov equations with the BSk24 equation of state (EOS), not accounting for (small) thermal corrections [20]. This EOS includes consistent crust and core regions and matches well with observational constraints from gravitational waves from binary-mergers, maximum-mass observations of pulsars, phase-coherent X-ray spectra mapped by the Neutron Star Interior Composition Explorer Mission (NICER), and other channels [26]. At the magnetic field strengths and temperatures considered here, such a cold and unmagnetised EOS is an excellent approximation. A spherically-symmetric star is assumed, ignoring rotational oblateness and/or magnetic deformations to the mass-density. Both could, in principle, influence the evolution (at least at early times) and introduce complicated anisotropies into the crustal conductivity profiles by breaking spherical symmetry, but such effects are expected to be small.

Throughout we present results for a ‘canonical’ star with a mass of  $M = 1.4M_{\odot}$ , radius  $R = 12.426$  km, and crustal thickness of 0.86 km. Additionally, we incorporate superfluid and superconducting gaps [11] for neutrons and protons, respectively, as they play a crucial role in cooling timescales by influencing the heat capacity and neutrino emissivity. Thermal and electrical conductivities are computed using data from the IOFFE repository (<http://www.ioffe.ru/astro/conduct/>). For a discussion of all these microphysical ingredients, beyond that which we can adequately explore here, we refer the reader to a comprehensive review article [23].

Axisymmetric evolutions of magnetic fields are considered in this work, utilising a recent version of a 2D magneto-thermal code [47], which has been modified to suit our current needs. This code numerically integrates the induction and heat-diffusion equations simultaneously within the neutron star interior. We postpone the transition to 3D simulations for now, much more computationally demanding, which can be achieved with the recently-developed MATINS code [2, 7, 8].

At the outer crust, defined numerically by a mass-density of  $\rho = 10^{10}$  g cm $^{-3}$ , we impose a current-free condition. While this is not strictly consistent with our spindown model, where magnetospheric twists should be injected following failure events, it should not alter the bulk statistics in a way that qualitatively changes our conclusions (relative to other uncertainties; see below). For crust-confined models, we also enforce that the crust-core boundary defines a perfect conductor: this is reasonable since the core becomes isothermal on timescales much faster [36] than the ages ( $\sim$  Myr) we predict for ULPs. Note, however, that the core magnetic field may also evolve via ambipolar diffusion over relatively short timescales [19], which could distort the field near the crust-core interface and possibly launch waves into the crust on dynamical timescales [6].

We assume an initial, isothermal temperature of  $10^{10}$  K, typical of the end of the proto-stage when the star becomes transparent to neutrinos. Importantly, the outer layers (envelope and atmosphere) react on much shorter timescales and quickly reach radiative equilibrium due to their low density. Simulating cooling across all layers up to the stellar surface would be computationally demanding, as it requires resolving vastly different timescales on the same numerical grid. Instead, we adopt the ‘standard’ approach by matching to a pre-computed, stationary envelope as a boundary condition, linking the surface temperature  $T_s$  (which determines the outgoing blackbody emission) and the temperature  $T_b$  at the crust-envelope boundary. This  $T_s$ - $T_b$  relation, which depends primarily on the average opacity and the local gravity [16], serves as an outer boundary condition for the heat diffusion equation. We consider an iron envelope model, expected for isolated stars without a history of accretion. Note that an envelope composed of lighter elements will be *hotter* at early times (i.e., before photon cooling begins to dominate over neutrino emissions) than one made primarily of iron [12]. For an object like 1E 1613 (or Galactic magnetars), an envelope composed of lighter elements may better fit the X-ray luminosity [12].

### 1. Crustal failure criteria

Consider the (traceless) Maxwell stress tensor [23]

$$M_{ij} = \frac{1}{4\pi} \left( B_i B_j - \frac{1}{3} B^2 \delta_{ij} \right). \quad (\text{A1})$$

According to a von Mises-like criterion under a Hookean stress-strain relation, the crust fails when the absolute value of the deviation from equilibrium exceeds some threshold,

$$\Delta M = |M_{ij} - M_{ij}^{\text{eq}}| \geq \sigma^{\text{max}}, \quad (\text{A2})$$

for local stress limit  $\sigma^{\text{max}}$ . These stresses are tracked throughout the simulations with event properties recorded when (A2) is met at any given spatial location and time step ( $\sim 0.1$  yr). To determine the energetics of an event, we integrate the square of the relative difference between the magnetic field at the failure time and the reference state, defined as the field at the start of the current equilibrium epoch (i.e., defining  $M_{ij}^{\text{eq}}$  just after the previous failure).

The critical stress threshold for crustal failure remains somewhat uncertain, as does the actual failure mechanism itself (see main text and below). If the crust behaves as a body-centred crystal, molecular dynamics [10] simulations indicate that

$$\sigma^{\text{max}} \approx \left( 0.0195 - \frac{1.27}{\Gamma - 71} \right) n_i \frac{Z^2 e^2}{a}, \quad (\text{A3})$$

for Coulomb parameter  $\Gamma$  (electrostatic-to-thermal energy ratio), atomic charge  $Z$ , ion-number density  $n_i$ , and where  $a$  is the typical inter-nuclear distance ( $\propto n_i^{-1/3}$ ). The affected region readjusts to a new equilibrium, resolidifies, and then resumes its elastic response, accumulating stress until another rupture [22, 33]. Failures can avalanche as adjacent regions exceeding a threshold ( $\Delta M \geq \epsilon \sigma^{\text{max}}$ ) become unstable following an event, possibly at sites determined by the crests of Hall or thermo-plastic waves [3].

Based on prior investigations [11, 33], the range  $0.8 \lesssim \epsilon \lesssim 1$  could be considered physical; we fix  $\epsilon = 0.85$ . In general, higher values increase event frequency but reduce affected areas, while lower values lead to larger but more infrequent failures. We do not expect that such changes would qualitatively adjust our findings here, since we are primarily interested in the global energetics of events, at least as far as spindown is concerned (see Fig. 5). For deformed crystals or more complicated structures, the threshold (A3) is expected to decrease and thus its use here implies an underestimate of the failure rate and overestimate of individual energies. While such adjustments are degenerate with the parameter  $\epsilon$  to some degree, meaning that a lower threshold should roughly correspond to a more malleable crystal, it is difficult to quantitatively estimate how the two relate. Note also that the threshold may instead increase significantly in ‘pasta’ regions (i.e., nonspherical configurations of nuclei, as related to the inter-nuclear distance introduced above), although this is unimportant as failures seldom occur in deeper regions. In fact, the majority of failures found in our simulations occur in the outermost layers ( $r \gtrsim 0.98R$ ).

For transparency, we note that there are also some important caveats worth highlighting with respect to our models. Probably most importantly, there is no strict inclusion of elasticity or plasticity: failures are handled through an instantaneous, von Mises mechanism where the crust heals prior to the next time-step without undergoing any lateral motions. Having the crust reset instantly is not really consistent with the radio-activation picture, since the zone should remain plastic for multiple time steps (and hence not accumulate stress) to account for a non-negligible duty cycle [8]. Moreover, not treating Lagrangian stresses consistently and the subsequent viscous response in this sense may lead to significant changes in the predicted failure statistics [6, 13]; our quantitative results should thus be treated with some degree of caution. In particular, while we have used the von Mises criterion to determine failure sites, molecular dynamics simulations instead indicate that a more physical mechanism is the Zhurkov model [10], where failures occur when thermodynamic fluctuations exceed a threshold energy over finite time intervals. This leads to gradual deformations rather than immediate failures and is more appropriate for modelling elastic/plastic transitions, though is difficult to handle numerically owing to the timescales of the problem. Nevertheless, because we cannot observa-

tionally infer the crustal field strength, it is likely that changes to our initial conditions could counter any such adjustments (e.g., the energetics scale directly with the magnetic energy stored in the failure volume).

On the other hand, we do not siphon out magnetic energy or inject heat into the crust following failures, which leads to overestimates of event rates as the Reynolds number will decrease locally in hotter or weaker-field regions (see Fig. 2). This is likely to significantly impact on CC models but should not seriously affect CT ones unless the failure-to-heat conversion ratio  $\gg \bar{\zeta}$  (see Fig. 5). Studies of these aspects in future would be important to validate the scenario put forward here (or otherwise).

## Appendix B: Relevant properties of isolated ULPs

Since ULPs form our main focus here and data have been used in the main text to support the ‘late-bloomer’ position, we provide here some details of relevant properties. Table I gives X-ray upper limits ( $L_X^{\text{max}}$ ), spin period, period derivative, estimated duty cycles, and distances, respectively, for nine ULPs that are not known to have binary companions.

Note that PSR J0901–4046 and 1E 161348–5055 (1E 1613) may or not be considered ULPs, the former because of its relatively low spin period ( $P \sim 76$  s) and the latter because no radio activity has been observed. On the other hand, 1E 1613 exhibits a high and variable X-ray luminosity spanning  $\sim 10^{33}$  erg/s to  $\sim 10^{35}$  erg/s indicative of ongoing heating despite showing a period of many hours. Whether the observed periodicity is, in fact, the spin period is less clear in this case though. The inferred period could, for instance, be tied to the precession period if the star undergoes free wobbles due to a strong toroidal field inducing a prolate deformation [24]; it is not uncommon for radio-quiet, young magnetars to display modulations at periods of many hours in pulsed X-ray components [16].

Another object deserving of individual discussion is CHIME J0630. The low DM ( $\approx 22.5$  pc cm $^{-3}$ ) of this source indicates it may be as close as [14]  $\gtrsim 90$  pc. This effectively rules out a dwarf and a disk interpretation due to the absence of optical, NIR, and UV counterparts [34]. Interestingly, trace contents of the radioactive iron nuclide  $^{60}\text{Fe}$  found in deep-sea archives of Earth’s oceans reveal interstellar influxes some time between 1.5 and 3.2 Myr ago from nearby supernovae [48]. Such an age fits naturally within the context of models presented here for DA J1832. On the other hand, pulse timing from CHIME J0630 indicates a period of only  $P \sim 7$  min, suggestive of inefficient failure-to-spindown conversions; this can be accommodated within our model for  $\zeta \lesssim 8 \times 10^{-4}$  (see Fig. 6). Owing to its proximity, this object should be prioritised for X-ray monitoring where even shallow bursts should be visible.

GPM J1839 has tight period derivative constraints [31] ( $\dot{P} \lesssim 3.6 \times 10^{-13}$  ss $^{-1}$ ) spanning the last  $\sim 3$  decades set

while the source was intermittently radio-loud. Owing to the mild constraints on this source’s X-ray luminosity (see Fig. 3), shallow failures triggering radio activity remain plausible provided the present-day field is comparatively weak ( $\lesssim 10^{14}$  G) and that the bulk of the enhanced spindown occurred prior to the present observations when the magnetoelastic energy reservoir was more plentiful. Even weaker fields than this could be (borderline) sufficient to sustain radio activity following failures [8].

### 1. DA J1832 activity timeline and alternative scenarios

Aside from ULPs generally, we have focussed on DA J1832 which has displayed both X- and radio-band activity simultaneously. We provide here a brief summary of the observational timeline and how we have interpreted it theoretically, providing also some caveats and alternative interpretations.

The sky surrounding DA J1832 has been regularly monitored over the last  $\sim$  decade because of the coincident position of a supernova remnant (SNR), G22.7–0.2. No pulsations had ever been recorded, despite  $\sim 6000$  hours of archival data having been accumulated by the Very Large Array since 2017. Radio pulses at a consistent period of  $P = 2656.247$  s (derivative upper limit  $\dot{P} < 10^{-9}$  ss $^{-1}$ ) were subsequently detected by the Australian SKA Pathfinder (ASKAP) with brightness  $\approx 1.9$  Jy on 8 December 2023. The source was highly variable (spanning  $\sim 20$  mJy to 18 Jy) through to February 2024 at frequencies ranging from  $\approx 0.3$  to 3 GHz, at which time a serendipitous X-ray search by Chandra measured an unabsorbed flux of  $\sim 5 \times 10^{-13}$  erg s $^{-1}$  cm $^{-2}$  in the 1–10 keV band, showing no signs of decay during the 20 ks over which photons were accumulated. The dispersion measure,  $\text{DM} \approx 458 \pm 14$  pc cm $^{-3}$ , indicates a distance of  $d = 4.5_{-0.5}^{+1.2}$  kpc based on the recent electron map models [29] and foreground gas measurements, and thus a peak luminosity of  $L_X \sim 10^{33}$  erg s $^{-1}$  for a hydrogen column density of  $N_{\text{H}} = 1.8 \times 10^{22}$  cm $^{-2}$  (note, however, there are non-trivial uncertainties on this value [14]). Spectral fits support a power-law component together with a  $\gtrsim$ keV hotspot of notably small radius,  $\lesssim 100$  m. Followup searches in August 2024 by Chandra and the Einstein Probe placed upper limits of  $L_X \lesssim 7 \times 10^{31}$  erg s $^{-1}$ , though the source remained radio-loud albeit dim through September 2024 at  $\sim 60$  mJy.

Note in particular that X-ray data were unavailable during the onset of radio pulsing in December 2023. Although one could take the observations at face value (see below), since the absence of evidence is not evidence of absence we have instead hypothesised the following: a (sub)-crustal event took place around the start of December 2023, which was directly responsible for radio activation by injecting magnetospheric twist or initiating a plastic flow. Thermoplastic heating [3] or particle

backflow [3] generated a localised hotspot surrounding the failure site as the twist ramped before decaying in the  $\lesssim$  months following February 2024. A schematic illustrating this scenario is depicted in Fig. 1, while a summary of relevant source parameters are listed in Tab. II.

Interestingly, it has been suggested [25] that there is an association between SNR G22.7–0.2 and DA J1832. However, this seems improbable [49] because (i) Sedov-Taylor theory of expansion predicts an age of  $\sim 25$  kyr, while (ii) for such an age, the location of DA J1832 indicates it must have been travelling some  $\sim 400$  km/s since birth (i.e. natal kick) but (iii) VLBI measurements (possible because of the multi-instrument radio detections) place an upper limit of  $\sim 190$  km/s. Even ignoring troubles with age therefore, one can likely discount this association.

Aside from this, the minimal timeline model considered in Fig. 1 and above does not take the observations at face value: the source started pulsing in radio in November 2023, exhibited heightened X-ray activity in February 2024, and then shut-off in X-rays quickly but continued pulsing for a while in radio. Such a model is, however, unusual for magnetars: almost always there is a burst *before* radio activation, though in some rare cases (two objects only; 1E 1547.0–5408 in 2022 and PSR J1119–6127 in 2016) radio activity is shut off some *weeks* prior to a (relatively weak) outburst [1, 27]. In these latter objects, however, it is plausible there was still crustal activity that went undetected due to the high baseline X-ray flux from the sources and so perhaps they are, in fact, not unusual.

Envisioning a situation where the source turns on in radio and then only becomes X-ray visible appears to require a magnetospheric origin where the field geometry becomes conducive to radio pulsing through some instability or other means, such as reconnection due the ‘diocotron’ instability [21] – an analogue of Kelvin-Helmholtz in collisionless plasmas – in a differentially rotating magnetosphere. One may imagine then that there is a back-reaction realised at the surface such that local and some global heating occurs which then dissipates faster than the magnetospheric twist. This could, in principle, source radio activation *followed* by X-rays, with persistent but waning radio as observed.

This however, appears difficult from an energetics perspective. The area of a spot produced due to backflow can be parameterised as

$$A = \pi R^2 u, \quad (\text{B1})$$

where  $u$  effectively determines the size of the current-carrying bundle where particles are created due to enhanced twist. For DA J1832 with a spot of size  $\sim 100$  m we have  $u \sim 10^{-4}$ . The anticipated luminosity of the spot due to kinetic heating reads [2]

$$L \approx 1.3 \times 10^{28} \times B_{14} R_6 \psi V_9 u^2 \text{ erg s}^{-1}, \quad (\text{B2})$$

where  $V_9$  is a threshold voltage (in units of  $10^9$  V), defined as the value of the electrostatic potential  $\Phi_e$  whereupon

copious particle supply is available to carry large currents, and  $\psi$  denotes the toroidal twist. The luminosity decay timescale in this picture reads [2]

$$t_{\text{ev}} \sim -\frac{L}{dL/dt} \approx 15 \times V_9^{-1} B_{14} R_6^2 \psi u \text{ yr}, \quad (\text{B3})$$

Matching to observations with  $t \sim 6$  months to eliminate  $V_9$  gives a maximum luminosity of

$$L_{\text{max}} \sim 10^{26} \times B_{14}^2 \text{ erg s}^{-1}, \quad (\text{B4})$$

even for ultra-strong fields, the luminosity is  $\sim 7$  orders too low to match observations of DA J1832. This allows us to exclude a backflow heating model triggered by magnetospheric bombardment. More generally, however, as magnetospheric (Alfvén) timescales are very short relative to those inside the star, it seems difficult to accept such a lengthy delay in radio- and X-ray activity – considerably longer than from any known magnetar [27] – is seeded by some instability in this case. One may also anticipate radio activity more akin to fast radio bursts (FRBs) rather than ongoing pulsations in such a case [15].

We remark, however, that ULP magnetospheres may be highly dynamical, as anticipated from the state-switching system [5] A J1935. Such aspects also impact on duty cycle estimates: a fixed latitude may be an unreliable estimator for inclination-related constraints on the probability of detection if the magnetosphere regularly alternates between states [27].

### Appendix C: Burst-to-spindown efficiencies

To provide some context for the value of  $\bar{\zeta} \sim 10^{-3}$  chosen in the main text (equation 4), we consider some relevant observations and theoretical elements here.

We first point out that, regrettably, the failure energy – that which is accessible from a simulation standpoint – is not directly observable and must instead be inferred from X-ray data. Such an intermediate conversion factor between (magneto-)elastic and outburst energies may be small; global simulations [5] of pulsar quakes where the crust and core are coupled – as appropriate to CT models – suggest that  $\sim 1\%$  of the quake energy escapes as observable radiation. For magnetars, the quake-to-radiation ratio may be higher as the ambient magnetic field mitigates thermodynamic losses: theoretical calculations of the crust-to-magnetosphere transmission coefficient [4, 18, 26, 28] suggest it scales with the field strength at high frequencies, especially in cases where the affected region liquifies.

Consider now some observations of bursts of relatively low luminosity – more appropriate for ULPs than giant flares and global events – from magnetars. For instance, 1E 1547.0–5408 released an X-ray burst in 2022; integrating the event light curve, the total burst energy can be estimated [25] as  $1 \lesssim E_X / (10^{41} \text{ erg}) \lesssim 6$  accounting for

uncertainties on column density and distance. Relative to the ‘baseline’ spindown rate of  $\dot{\nu} = -3.63(3) \times 10^{-12} \text{ s}^{-2}$ , an *average* net increase of  $|\delta\dot{\nu}| \approx 2.54 \times 10^{-12} \text{ s}^{-2}$  was observed [27] over  $\approx 147$  days following the event, roughly translating into an excess rotational kinetic energy loss of  $\gtrsim 3 \times 10^{41} \text{ erg}$ . For this, possibly extreme, event we could thus anticipate  $\bar{\zeta} \sim \mathcal{O}(10^{-2})$ . Perhaps more appropriate for ULPs, GPM J1839–10 exhibits linear-to-circular polarisation [31] conversion in a way that is remarkably reminiscent of XTE J1810–197, suggesting their magnetospheric environments may be alike. The latter magnetar is known to enter into epochs of enhanced spindown post outburst. Following its 2003 event(s),  $\dot{\nu}$  increased by a factor  $\approx 6$  that stabilised over the next  $\sim 3$  years [6]. Spindown remained relatively steady until 2018 when the source burst again, with an average increase of  $\delta\dot{\nu}/\dot{\nu} \approx 2.5$ ; pulsed fraction differences point towards different emission geometries between events [7], which could be responsible for the discrepancy in  $\delta\dot{\nu}$  increases across events. The burst energy can be further estimated [7] as  $\sim (4 \pm 2) \times 10^{42} \text{ erg}$  while the source lost  $\sim 10^{41} \text{ erg}$  of rotational kinetic energy, suggesting  $\bar{\zeta} \sim \mathcal{O}(10^{-3})$ . An upper limit of  $\bar{\zeta} \sim \mathcal{O}(10^{-2})$  could be defended in some (possibly rare) cases if ULPs behave more like 1E 1547.0–5408.

With respect to simulations presented in the main text, we have enforced  $\dot{P} < 10^{-9} \text{ ss}^{-1}$  for DA J1832. While the object may have been spinning down faster in prior unobserved epochs, especially at early times, this keeps with our conservative approach. It would be straightforward however to relax such a condition and instead impose a maximum  $\dot{P}$  from, say, a split-monopole magnetosphere for which the spindown is maximum for a given  $B_p$ . GPM J1839–10, for example, has a present-day bound of  $\dot{P}_{\text{GPMJ1839}}^{\text{max}} < 3.6 \times 10^{-13} \text{ ss}^{-1}$  which would imply a minimum age of  $\sim 100 \text{ Myr}$  if  $P < \dot{P}_{\text{GPMJ1839}}^{\text{max}}$  at all times which is too long to stall decay for even CT models.

In continuing the topic of  $\dot{P}$  enhancement, we discuss briefly an alternative mechanism that may be at work in spinning down some stars. Indeed, while ULPs have long periods, they may not be the slowest known neutron stars. For example, the X-ray binary 4U 1954+319 has a spin period [30] of  $\gtrsim 5 \text{ hours}$ . Spindown in such systems is intensified by propeller torques due to the accretion

flow in epochs when the Alfvén radius ( $R_A$ ) – where material is force stopped – exceeds the corotation radius ( $R_{\text{co}}$ ) of circling plasma. While interactions with a fallback disk surviving the supernova are often invoked to explain ULP periods, this may be difficult to engineer from theoretical expectations. The optimal situation from a spindown perspective [40] is that of prolonged fallback with rate  $\dot{M} \gtrsim 10^{-10} M_{\odot} \text{ s}^{-1}$ .

However, the fallback timescale  $t_{\text{fb}} \sim (G\bar{\rho})^{-1/2}$  for mean disk mass-density  $\bar{\rho}$  is limited by the progenitor envelope: an upper limit of  $t_{\text{fb}} \sim \text{months}$  is realised for red supergiants [32] ( $\bar{\rho} \sim 10^{-7} \text{ g cm}^{-3}$ ) where  $\dot{M} \gtrsim 10^{-8} M_{\odot} \text{ s}^{-1}$ . Even ignoring the effects of magnetic burial [17, 43], we thus anticipate [10]

$$\frac{R_A}{R} \sim 8 \left( \frac{\dot{M}}{10^{-8} M_{\odot} \text{ s}^{-1}} \right)^{-2/7} \left( \frac{B}{10^{14} \text{ G}} \right)^{4/7}, \quad (\text{C1})$$

and, as propeller torques are only active when

$$R_A > R_{\text{co}} \sim 170R \times \left( \frac{P}{1 \text{ s}} \right)^{2/3}, \quad (\text{C2})$$

reaching long periods appears difficult.

Moreover, fallback disks should reveal themselves via outflows in either the X- or optical bands [34], the signatures of which have not been confidently detected around any star to date. Even if lower and sustained fallback rates are realised in Nature without having the low-density material be ablated, a disk model does not help to explain the radio activation and late-time X-ray activity of DA J1832. By contrast, we have demonstrated that appealing to external mechanisms is not necessary to explain the spins or other characteristics of ULPs, making the model more attractive from an Occam’s razor perspective. Nevertheless, for the hot ( $L_X \lesssim 10^{35} \text{ erg s}^{-1}$ ) and slow ( $P \lesssim 7 \text{ hour}$ ) object 1E 1613, a disk has the obvious advantage that the source may remain hot, which is difficult to accommodate in the context of our results (Fig. 3). If a disk is present, an interesting possibility is that cyclotron resonant scattering features may be detectable in future, which can be used to directly probe the magnetospheric field strength and could confirm magnetar nature for energetic line profiles.

[1] Archibald R. F., Burgay M., Lyutikov M., Kaspi V. M., Esposito P., Israel G., Kerr M., et al., 2017, *ApJL*, 849, L20. doi:10.3847/2041-8213/aa9371

[2] Ascenzi, S., Viganò, D., Dehman, C., Pons, J. A., Rea, N. & Perna, R. 3D code for magneto-thermal evolution in isolated neutron stars, MATINS: thermal evolution and light curves. *Mon. Not. R. Astron. Soc.* **533**, 201–224 (2024).

[3] Beloborodov, A. M. & Li, X. Magnetar heating. *Astrophys. J.* **833**, 261 (2016).

[4] Caleb M., Heywood I., Rajwade K., Malenta M., Stappers B. W., Barr E., Chen W., et al., 2022, *NatAs*, 6, 828. doi:10.1038/s41550-022-01688-x

[5] Caleb M., Lenc E., Kaplan D. L., Murphy T., Men Y. P., Shannon R. M., Ferrario L., et al., 2024, *NatAs*, 8, 1159. doi:10.1038/s41550-024-02277-w

[6] Camilo, F., Ransom, S. M., Halpern, J. P., Alford, J. A. J., Cognard, I., Reynolds, J. E., Johnston, S., Sarkissian, J. & van Straten, W. Radio disappearance of the magnetar XTE J1810-197 and continued X-ray

- timing. *Astrophys. J.* **820**, 110 (2016).
- [7] Dehman, C., Viganò, D., Pons, J. A. & Rea, N. 3D code for magneto-thermal evolution in isolated neutron stars, MATINS: the magnetic field formalism. *Mon. Not. R. Astron. Soc.* **518**, 1222–1242 (2023).
- [8] Dehman, C., Viganò, D., Ascenzi, S., Pons, J. A. & Rea, N. 3D evolution of neutron star magnetic fields from a realistic core-collapse turbulent topology. *Mon. Not. R. Astron. Soc.* **523**, 5198–5206 (2023).
- [9] De Luca A., Caraveo P. A., Mereghetti S., Tiengo A., Bignami G. F., 2006, *Sci*, 313, 814. doi:10.1126/science.1129185
- [10] Glampedakis, K. & Suvorov, A. G. Modelling spin-up episodes in accreting millisecond X-ray pulsars. *Mon. Not. R. Astron. Soc.* **508**, 2399–2411 (2021).
- [11] Ho, W. C., Elshamouty, K. G., Heinke, C. O. & Potekhin, A. Y. Tests of the nuclear equation of state and superfluid and superconducting gaps using the cassiopeia a neutron star. *Phys. Rev. C* **91**, 015806 (2015).
- [12] Hyman S. D., Wijnands R., Lazio T. J. W., Pal S., Starling R., Kassim N. E., Ray P. S., 2009, *ApJ*, 696, 280. doi:10.1088/0004-637X/696/1/280
- [13] Kojima Y., 2024, *ApJ*, 974, 125. doi:10.3847/1538-4357/ad7382
- [14] Lattimer, J. M. & Steiner, A. W. Neutron star masses and radii from quiescent low-mass X-ray binaries. *Astrophys. J.* **784**, 123 (2014).
- [15] Lyubarsky Y., 2020, *ApJ*, 897, 1. doi:10.3847/1538-4357/ab97b5
- [16] Makishima K., Enoto T., Hiraga J. S., Nakano T., Nakazawa K., Sakurai S., Sasano M., et al., 2014, *PhRvL*, 112, 171102. doi:10.1103/PhysRevLett.112.171102
- [17] Melatos, A. & Priymak, M. Gravitational radiation from magnetically funneled supernova fallback onto a magnetar. *Astrophys. J.* **794**, 170 (2014).
- [18] Most, E. R., Kim, Y., Chatziioannou, K. & Legred, I. Nonlinear Alfvén-wave dynamics and premerger emission from crustal oscillations in neutron star mergers. *Astrophys. J. Lett.* **973**, L37 (2024).
- [19] Passamonti A., Akgün T., Pons J. A., Miralles J. A., 2017, *MNRAS*, 465, 3416. doi:10.1093/mnras/stw2936
- [20] Pearson, J. M. *et al.* Unified equations of state for cold non-accreting neutron stars with Brussels-Montreal functionals - I. Role of symmetry energy. *Mon. Not. R. Astron. Soc.* **481**, 2994–3026 (2018).
- [21] Pétri, J. Theory of pulsar magnetosphere and wind. *J. Plasma Phys.* **82**, 635820502 (2016).
- [22] Pons, J. A. & Perna, R. Magnetars versus high magnetic field pulsars: a theoretical interpretation of the apparent dichotomy. *Astrophys. J.* **741**, 123 (2011).
- [23] Potekhin, A. Y., Pons, J. A. & Page, D. Neutron Stars—Cooling and Transport. *Space Sci. Rev.* **191**, 239–291 (2015).
- [24] Suvorov A. G., Kokkotas K. D., 2021, *MNRAS*, 502, 2482. doi:10.1093/mnras/stab153
- [25] Suvorov, A. G. The radio shut-off, glitch, and X-ray burst in 1E 1547.0-5408 interpreted through magnetic reconfiguration. *Mon. Not. R. Astron. Soc.* **523**, 4089–4096 (2023).
- [26] Suvorov, A. G., Kuan, H.-J. & Kokkotas, K. D. Premerger phenomena in neutron star binary coalescences. *Universe* **10**, 441 (2024).
- [27] Timokhin A. N., 2010, *MNRAS*, 408, L41. doi:10.1111/j.1745-3933.2010.00924.x
- [28] Tsang, D., Read, J. S., Hinderer, T., Piro, A. L. & Bondarescu, R. Resonant shattering of neutron star crusts. *Phys. Rev. Lett.* **108**, 011102 (2012).
- [29] Yao, J. M., Manchester, R. N. & Wang, N. A new electron-density model for estimation of pulsar and FRB distances. *Astrophys. J.* **835**, 29 (2017).

## ACKNOWLEDGEMENTS

We thank Alex Cooper for discussions on pulsar activity sourced by plastic flow. We gratefully acknowledge the support provided by the Conselleria d'Educació, Cultura, Universitats i Ocupació de la Generalitat Valenciana through Prometeo Project CIPROM/2022/13 and grant ASFAE/2022/026 (with funding from NextGenerationEU PRTR-C17.I1), and from the AEI grant PID2021-127495NB-I00 funded by MCIN/AEI/10.13039/501100011033. CD acknowledges MINISTERIO DE CIENCIA, INNOVACIÓN Y UNIVERSIDADES Organismo/s cofinanciador/es: AGENCIA ESTATAL DE INVESTIGACIÓN, UNIÓN EUROPEA (FSE+) Y UNIVERSIDAD DE ALICANTE. Her contract is part of fellowship JDC2023-052227-I financiado por MCIU/AEI/10.13039/501100011033 y por el FSE+.

## AUTHOR CONTRIBUTIONS

The first two authors of this work (C. Dehman and A.G. Suvorov) contributed significantly to the conceptualisation, implementation, model design, writing, and editing: to that degree it is with regret that lead authorship cannot be more perceptibly shared. Their contributions were distinct but approximately equal (e.g., A.G. Suvorov handled spindown elements and C. Dehman conducted the magnetothermal simulations and formulated the corresponding results presented in this manuscript, with ongoing mutual feedback). J. Pons was also directly involved in matters of editing, presentation, and physics discussions regarding the key properties of the model(s) and simulation setup(s).

TABLE I. Relevant details for a variety of isolated ULPs, namely upper limits on the X-ray luminosity ( $L_X^{\max}$ ), the observed pulse period ( $P$ ; in descending order) and its (upper-limit) derivative ( $\dot{P}^{\max}$ ), together with estimated duty cycles ( $D$ ) and distances ( $d$ ). Additional details on DA J1832 are provided in Table II. Some object names have been shortened (see text).

Name	$L_X^{\max}$ (erg/s)	$P$ (s)	$\dot{P}^{\max}$ (s/s)	$D$ (%)	$d$ (kpc)
PSR J0901–4046* [4]	$2 \times 10^{30}$	75.88554711(6)	$2.25(1) \times 10^{-13}$	0.7	0.39(6)
CHIME J0630 [14]	$\sim 1 \times 10^{29}$	421.35542(1)	$1.6 \times 10^{-12}$	$\lesssim 0.8$	0.17(8)
GX J1627 [39]	$2 \times 10^{30}$	1091.1690(5)	$1.2 \times 10^{-9}$	$< 5$	1.3(5)
GPM J1839–10 [20, 31]	$2 \times 10^{33}$	1318.1957(2)	$3.6 \times 10^{-13}$	$\lesssim 22.7$	5.7(2.9)
DA J1832 <sup>§</sup> [25, 49]	$\sim 10^{33}$	2656.247(1)	$9.8 \times 10^{-10}$	$< 10$	4.8(0.8)
A J1935 [5]	$4 \times 10^{30}$	3225.309(2)	$\lesssim 2.7 \times 10^{-10}$	1.5	4.9(5)
GCRT J1745–3009* [12]	$\lesssim 2 \times 10^{34}$	4620.72(1.26)	–	13	$\sim 8(?)$
A J1839 [24]	$10^{33}$	23221.7(1)	$1.6 \times 10^{-7}$	$\lesssim 3.1$	4.0(1.2)
1E 1613 <sup>#</sup> [9]	$> 10^{33}$	24030(108)	$1.6 \times 10^{-9}$	0(?)	3.9(8)

**Notes.** For each source, X-ray limits are quoted assuming the mean distance and ‘typical’ hydrogen column densities, as per the references, at one digit of precision to roughly account for uncertainties. \* For PSR J0901 there is a decisive  $\dot{P}$  measurement rather than only an upper limit. § Observed X-ray luminosity during outburst (upper limit  $\lesssim 5 \times 10^{31}$  erg in quiescence). \* No period derivative constraints are available. # Depending on classification, 1E 1613 may not be considered a ULP as it has never displayed radio pulsations; for this object there is also consistent X-ray detections, revealing a volatile source whose  $L_X$  varied by two orders of magnitude between years of observations spanning 1990 to 2004.

TABLE II. Summary of relevant observed properties [25, 49] of DA J1832. Here we have introduced the radio flux density  $S_\nu$ , the considerable variation of which may be attributable to a waning twist or magnetospheric pollution from fireball plasma.

Observed/derived properties	Value
Spin period ( $P$ )	$2656.247 \pm 0.001$ s
Period derivative ( $\dot{P}$ )	$< 10^{-9}$ ss <sup>-1</sup> (95%)
$L_X^{\text{quiescent}}$ (ca. 2011)	$< 5.3 \times 10^{31}$ erg/s ( $3\sigma$ )
$L_X^{\text{quiescent}}$ (Aug. 2024)	$< 6.5 \times 10^{31}$ erg/s ( $3\sigma$ )
$L_X^{\text{active}}$ (Feb. 2024)	$\sim 10^{33}$ erg/s
$S_\nu^{\text{quiescent}}$ (2017–2023)	$< 10$ mJy
$S_\nu$ (Dec. 2023)	$\sim 1$ Jy
$S_\nu$ (Feb. + Mar. 2024)	$\sim 10$ Jy
$S_\nu$ ( $\sim$ Sep. 2024)	$\sim 60$ mJy